2021-04

Wave Modulation of Flows on Open and Closed Reefs

Lindhart, M

Correspondence to:
M. Lindhart,
lindhart@stanford.edu

Wave Modulation of Flows on Open and Closed Reefs

M. Lindhart[1] , J. S. Rogers[1] , S. A. Maticka[1] , C. B. Woodson[2] , and S. G. Monismith[1]

[1]Bob and Norma Street Environmental Fluid Mechanics Laboratory, Department of Civil and Environmental Engineering, Stanford University, Stanford, CA, USA, [2]COBIA Lab, University of Georgia, Athens, GA, USA

Abstract Using observations, numerical models, and theory, we explore a framework to classify reefs as open or closed based on their dynamics. While the concepts of open and closed reefs are used widely in studies of coral reef hydrodynamics and are generally based on geometry, there is no consensus on what qualifies as open and closed. With observations from Ofu, American Samoa, we show that the reef flat exhibits two different dynamical regimes depending on tidal and wave forcing. Flow over this reef flat resembles a classic one-dimensional barrier reef flow during low tide, where wave setup creates a cross-reef pressure gradient which forces flow on the flat. On high tide, however, flow on the flat is oblique to the crest, and at times directed offshore. We reproduce this behavior in an idealized numerical model of a fringing reef. We classify open reefs as a condition where an onshore, wave-generated pressure gradient is balanced by friction, and closed reefs as a condition where an onshore radiation stress gradient is opposed by an offshore pressure gradient. Results from the fringing reef model show that the system transitions between open and closed behavior over a tidal cycle. Results from an additional barrier reef numerical model exhibits almost exclusively open reef behavior, for which we derive a simple theoretical model. We argue that classifying reefs as open or closed based on their dynamics, rather than geometry, is a more meaningful approach to comparing reefs and predicting their dynamical response to wave and tidal forcing.

Plain Language Summary The complicated variability in physical and biological characteristics of different coral reefs world-wide poses a challenge to explain observations on reefs. We investigate how flows on barrier reefs and fringing reefs differ, based on field observations from Ofu, American Samoa, and computer models. Two different reefs, subject to the same forcing from waves and tides, might respond very differently based on their physical characteristics such as geometry and roughness. Using computer models, we present a fringing and barrier reef and show that they can exhibit two limiting types of dynamic: Either they are similar to open channel flow, or they are similar to flow observed on beaches. While the barrier reef showed open channel flow consistently, the fringing reef transitioned from open channel flow on low tide to beach flow on high tide, or what we here call open and closed behavior. Understanding the classification of a reef can aid in predicting how a reef will respond to changes in forcing such as storms and sea level rise.

1. Introduction

Flows on coral reefs are forced by waves, tides, and winds (Monismith, 2007). The effect of waves on the mean flow momentum balance was described by Longuet-Higgins and Stewart (1964), who introduced the concept of a radiation stress gradient. Energy is dissipated as waves break on sloping beaches and reefs, and the resulting onshore radiation stress gradient is balanced by an offshore pressure gradient, creating wave setup. On a reef flat with a deeper lagoon behind it, wave setup drives a flow across the reef and into the lagoon (Gourlay, 1996a; Symonds et al., 1995). The mechanism of wave setup on submerged reefs can lead to remarkable dynamics, for example, Callaghan et al. (2006) who described two South Pacific atolls where the water level always exceeded the ocean water level due to wave pumping.

While wave-driven flow is ubiquitous on shallow reefs with persistent waves, it is clear that not all reefs respond to wave forcing in the same way. To first order, the dynamical response depends on geometry (Gourlay, 1996b; Lowe et al., 2010, 2015), friction (Franklin et al., 2016; Lentz et al., 2016), wind (Atkinson et al., 1981; Hoeke et al., 2013; Sous et al., 2017), and tidal range (Bonneton et al., 2007; Gourlay, 1996a). Notable differences have been observed between what has loosely been termed "open reefs" and "closed reefs," although no definition of either has been settled upon. In general, an "open reef" is thought to be a

reef where the water level at the leeward side is largely unaffected by the reef dynamics (i.e., the water level is the same as the open ocean). "Closed reefs" describe reefs where the leeward water level is elevated and of similar magnitude to the setup on the reef itself. Meanwhile, the term "closed reef" is also used to describe a geometrically closed lagoon or pool surrounded by a fringing reef, connected to the open ocean through narrow channels. However, this geometric definition can be deceptive: For example, the reef-lagoon system on the northern shore of Moorea, French Polynesia looks closed. Nevertheless, there is little wave-driven setup in the leeward lagoon relative to the reef flat and the cross-reef flow is governed by a pressure gradient-friction balance; thus the system is effectively open (Monismith et al., 2013). In contrast, in Kaneohe Bay, which is geometrically similar to the Moorea system, wave-driven setup of the lagoon is nearly independent of position, and therefore, behaves like a closed system (Lowe et al., 2009). Hence, using the terms open and closed to describe both geometry and dynamics can be problematic. Moreover, not all reefs have associated lagoons, see for example, Lentz et al. (2016). Thus, it is more meaningful to create a definition based on the reef flow dynamics, rather than on the presence or absence of a lagoon or channels.

The goal of this work is to define a classification for wave-affected reefs as either open or closed based on the reef flat momentum balance. We define the reef flat as shallow, near-horizontal section of reef, downstream of the surf zone if waves are breaking. We find that these environments are governed by either a pressure gradient-friction balance (open channel flow) or by a pressure gradient-radiation stress gradient balance (beach dynamics). This definition can then be used as the basis for understanding the response of these two types of systems to incident wave forcing. On open reefs, an analytical model can explain variability of both phase and magnitude in the tidal variability in cross-reef flows. Closed reefs are more complex, and our numerical modeling results suggest that the parameter H_s/h_r, the ratio of the wave height to the depth on the reef, plays an important role in determining the cross-reef flow. On closed reefs we also find that waves force an alongshore flow that depends on the tidally varying water depth.

To illustrate a classification based on dynamics rather than geometry, we employ observations from Ofu, American Samoa, where an extensive field program was carried out in 2016–2017 (see Hefner et al., 2019; Maticka, 2019; Rogers et al., 2018). The Ofu reef is a shallow (0–2 m depth), fringing reef with small pools and narrow channels connecting the pools to the open ocean. Geometrically, the Ofu reef would be considered to be a closed reef, however, it behaves like an open reef on low tide and like a closed reef on high tide. To understand the dynamics of flows on this reef, we developed an idealized numerical model and studied cases of varying incident wave heights. We developed a second model with the same geometry and forcing, but without the leeward land mass – essentially a barrier reef – to represent an open reef. Here, we seek to understand the flow regimes of these two types of shallow coral reef that can be considered end members of the governing dynamics.

2. Theory of Wave-Driven Flow

The one-dimensional (1D) depth-integrated, wave-averaged momentum equation for a shallow reef in the cross-reef (x) direction is given by (Mei, 1983)

$$\frac{\partial (h + \overline{\eta})u^L}{\partial t} + \frac{\partial (h + \overline{\eta})(u^L)^2}{\partial x} = -g(h + \overline{\eta})\frac{\partial \overline{\eta}}{\partial x} - \frac{1}{\rho}\frac{\partial S_{xx}}{\partial x} - \frac{\tau_b}{\rho},$$

where $u^L = u + u^S$ is the depth-averaged, Lagrangian velocity in the x-direction, which is the sum of the Eulerian velocity u and the Stokes flow u^S. We will refer to the cross-reef, Eulerian, depth-averaged velocity on the reef flat and in the channel as u_r and u_{ch}, respectively. Furthermore, h is the still water depth on the reef flat, $\overline{\eta}$ is the wave setup, x is the cross-reef coordinate (see Figure 1), ρ is a reference water density, S_{xx} the cross-reef radiation stress. τ_b is the bed shear stress, which is often modeled with either a linear or quadratic dependence on the depth-averaged, Eulerian velocity. Here, we assume a quadratic bottom friction proportional to a drag coefficient C_D, $\tau_b = \rho C_D u|u|$. In the presence of strong wave-induced velocities relative to the mean flow, a linear friction term is sometimes used (Hearn, 1999; Lowe et al., 2009).

Wave breaking on the sloping fore reef establishes an onshore radiation stress gradient, which is opposed by an offshore pressure gradient, generating wave setup. Friction and advection can be important on the fore reef; advection is particularly important in the presence of steeply sloping reefs. On the near-horizontal
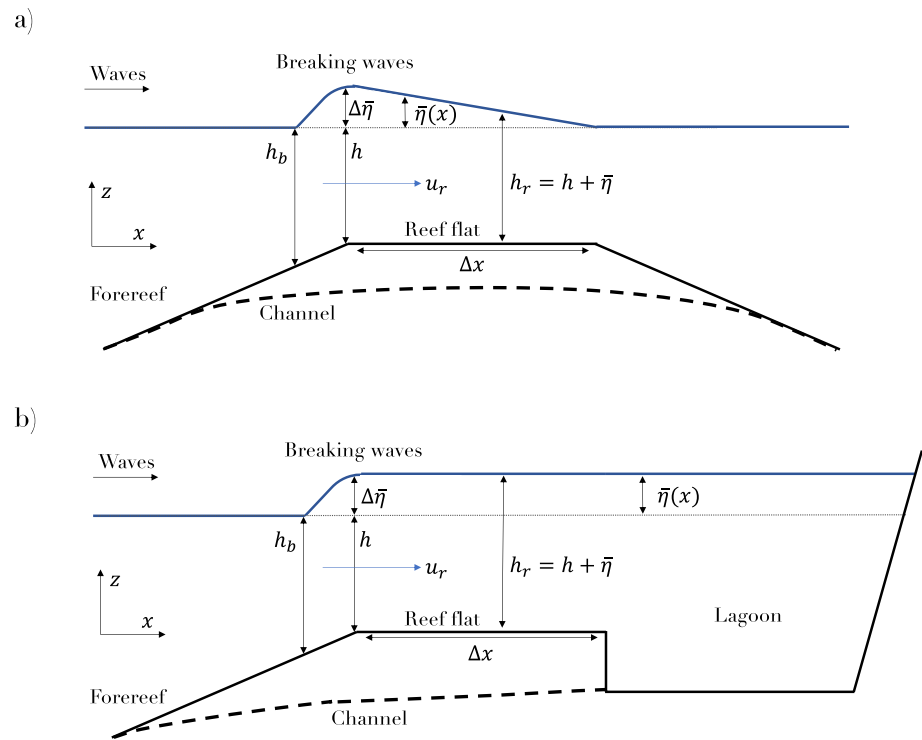
Figure 1. Idealized reef models. (a) Barrier reef. (b) Fringing reef.

reef flat, we assume advection is negligible in the absence of strong spatial variability. For a wave-averaged flow, the cross-reef dynamics on the reef flat are then determined by a balance between pressure gradients, radiation stresses gradients, and friction

$$-g(h + \bar{\eta})\frac{\partial \bar{\eta}}{\partial x} - \frac{1}{\rho}\frac{\partial S_{xx}}{\partial x} - \frac{\tau_b}{\rho} = 0. \tag{1}$$

The relative importance of these three terms vary depending on the site. If the governing momentum equation on the reef flat can be reduced to a balance between the pressure gradient and friction, we characterize this as open-reef dynamics. If, on the other hand, the momentum equation can be reduced to a balance between the pressure gradient and radiation stress gradient, we characterize it as closed-reef dynamics. Often, the maximum wave setup is assumed to be determined by a pressure gradient-radiation stress gradient balance (Tait, 1972), so that

$$\Delta \eta \approx \frac{1}{1 + 8 / (3\gamma^2)}(h_b - h_r) = \Gamma(h_b - h_r), \tag{2}$$

where h_b is the depth at breaking, and $h_r = h + \bar{\eta}$. In the simplest model of breaking, h_b is determined by the incident wave energy flux and by the breaking parameter

$$\gamma = H / h_b, \tag{3}$$

which is the ratio of the local wave height to the local depth when waves are breaking (Vetter et al., 2010). On beaches, γ is known to vary with beach slope and offshore wave steepness (Raubenheimer et al., 1996); on reefs, various values of γ have been found by matching setup to Equation 2 (Monismith et al., 2013; Vetter et al., 2010). Values of γ on reefs vary; Lowe et al. (2009) reported $\gamma = 0.3$ from Kaneohe Bay, Hawai'i, and Vetter et al. (2010) found $\gamma \sim 0.9$–1.1 in Ipan, Guam. While a single value of γ is often used for a given site, Becker et al. (2014) found that the breaking parameter γ itself can vary tidally.
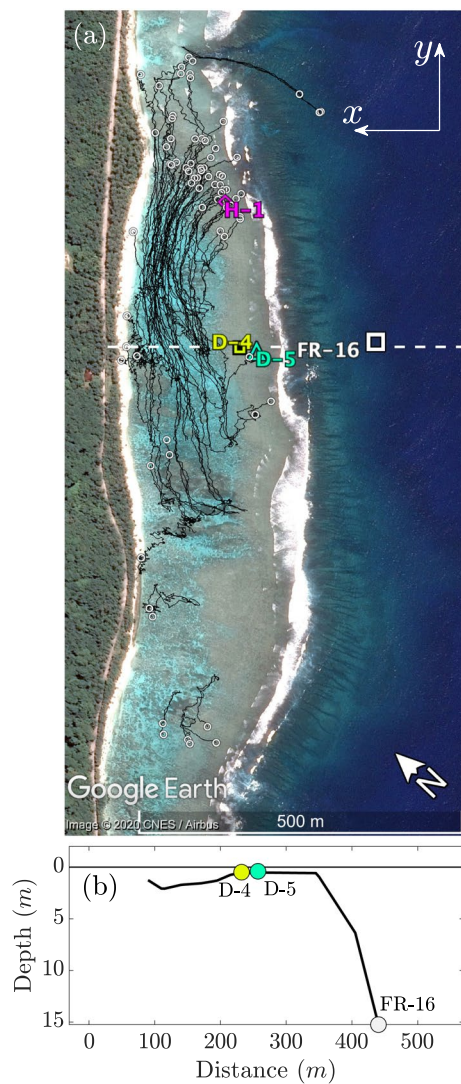
Figure 2. (a) Deployment overview from Ofu, American Samoa. Only instruments used in this paper are shown, see Maticka (2019) for full deployment details. Instruments and their sampling rates are given in Table 1. Black lines indicate drifter tracks with end points as white circles. White, dashed line shows location of bathymetry transect in (b). Map data: Google Earth, CNES/Airbus.

Finally, the numerical modeling we describe below is based on the breaking parameterization of Battjes and Janssen (1979) which extends the simple breaking model described by Equation 3 by accounting for non-monochromatic ocean waves (see also Thornton & Guza, 1983). The Battjes and Janssen (1979) breaking model also uses a limiting wave height defined by γ, but for a given value of γ this tends to produce different wave heights in the surf zone than the simple model. Moreover, while Vetter et al. (2010) assumed that breaking is localized, which may be a better physical description of breaking on reefs than is the model of Tait (1972) which assumes that Equation 3 describes the effects breaking everywhere on the fore reef, both approaches give the same result, that is, Equation 2. No such analytical result is possible for the Battjes and Janssen (1979) model. Thus, accurately modeling wave-driven flows on reefs may be limited by our ability to represent breaking on steep reef faces.

3. Observations From Ofu, American Samoa

A comprehensive field program was deployed in Ofu, American Samoa between March 10–28, 2017 (Figure 2; see Hefner et al., 2019; Maticka, 2019; Rogers et al., 2018). Instrument specifications, locations, and sampling schemes are listed in Table 1

Mean depth on the reef flat was about 0.6 m, with a 1 m tidal range (Figure 3). The significant wave height (H_s) on the fore reef varied between 0.5 and 1.3 m. The flow through the channel (Figure 3c) was always directed offshore, and showed clear variability with both wave height and tides, with stronger channel flow on high tide than on low tide. Due to instrument failure, we only have 5 days of observations from the reef flat itself. Figure 3d shows a quiver plot of depth-averaged velocities on the flat. During low tide, the cross-reef flow (u_r) on the reef flat is maximum and directed perpendicular to the reef crest. During high tide, the along-reef flow (v_r) is maximum, and directed at an angle to the reef crest, toward the channel. Occasionally on high tide, the flow reverses direction and is entirely offshore on the reef flat, shown as red vectors in Figure 3.

The directionality of the flow on the reef flat indicates a complicated two-dimensional flow structure, where the direction (perpendicular or at an angle to the crest) depends on the tide, and occasional flow reversal (offshore) occurs. While the magnitude of the channel flow is clearly proportional to offshore wave heights and tides, this correlation is not obvious on the reef flat. In Figure 4, we examine the variability of the cross-reef flow, the along-reef flow and the magnitude of the flow with wave height, depth on the reef flat, and the ratio of the de-shoaled, offshore equivalent wave height to the depth.

| **Table 1**				
Deployment Details				
Instrument	Location	Sampling rate	Duration	Mean depth
Teledyne vADCP	D-4: Reef flat	Continuous at 0.33 Hz, 3-cm bins	March 10–28, 2017	0.62 m
RBR SoloD	D-5: Reef flat	Continuous 1 Hz	March 10–28, 2017	0.55 m
SeaBird 26+	FR16: Fore reef	1024 burst samples at 2 Hz every 30 min	March 10–28, 2017	15 m
Teledyne vADCP	H-1: Channel	Continuous at 0.33 Hz, 3-cm bins	March 10–28, 2017	0.59 m
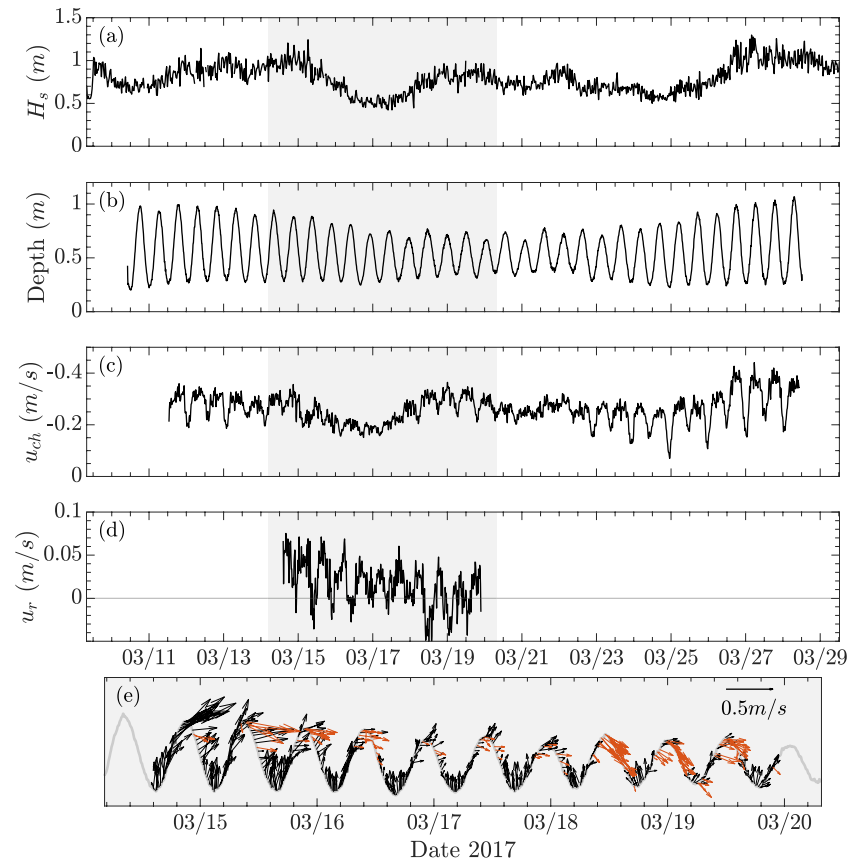
Figure 3. (a) H_s at FR16. (b) Depth at D-5. (c) Depth-averaged velocity at H-1, negative offshore out of the channel. (d) Cross-shore, depth-averaged velocity at D-4, positive onshore. (e) Quiver plot of depth-averaged velocities at D-4. Length of arrows indicate velocity magnitude, *x*-axis is aligned alongshore and *y*-axis is cross shore. The quiver plot is imposed on the tidal water level to indicate direction of flow changing with the tide. Black arrows have an onshore component, and red arrows have an offshore component. Figure (e) spans the period indicated in gray in figures (a)–(d).

Noting that our observations on the reef flat cover a short period of time and that we are looking at a relatively small parameter space, we can make provisional inferences about the nature of the flow. Contrary to classic 1D reef models, the cross-reef flow shows no correlation with wave heights. In particular, flow reversal (offshore) occurs at all but the largest wave heights recorded. Cross-reef flow correlates inversely with the depth, or proportional to H_s^{deep} / h_r. This is in agreement with our observations in Figure 3e, where we note that on low tide, the flow is directed onshore in the cross-reef direction, and reverses offshore on high tide. Similarly, v_r correlates clearly with the depth on the reef flat. On low tide, $v_r \approx 0$, whereas with increasing water depth, the flow deflects toward the channel (north-east). While neither the cross-reef nor the along-reef velocities seem correlated with the wave height, the magnitude of the flow does correlate with it (Figure 4g). Based on these observations, the magnitude of the flow on the reef flat is determined by the wave height, but the direction is determined by the tide.

The flow on the Ofu reef flat resembles the classic 1D reef model described by Symonds et al. (1995) on low tide, where the flow direction is perpendicular to the crest. This is consistent with an open reef. However, the oblique and occasionally reversed flow on high tide is not accounted for in these models, and is consistent with a closed reef. Hence, Ofu seems to occupy a transient position between the two end members of the governing dynamics. On low tide, the reef resembles an open reef, and on high tide it resembles a closed reef. To understand the dynamics of this reef geometry, we set up an idealized numerical model of the reef, which we will refer to as our fringing reef model. To compare to a truly open reef, we also create a model without the constriction of a shallow shoreward pool, which we refer to as our barrier reef model. Both models have periodic channel incisions, similar to the reef in Ofu, American Samoa.
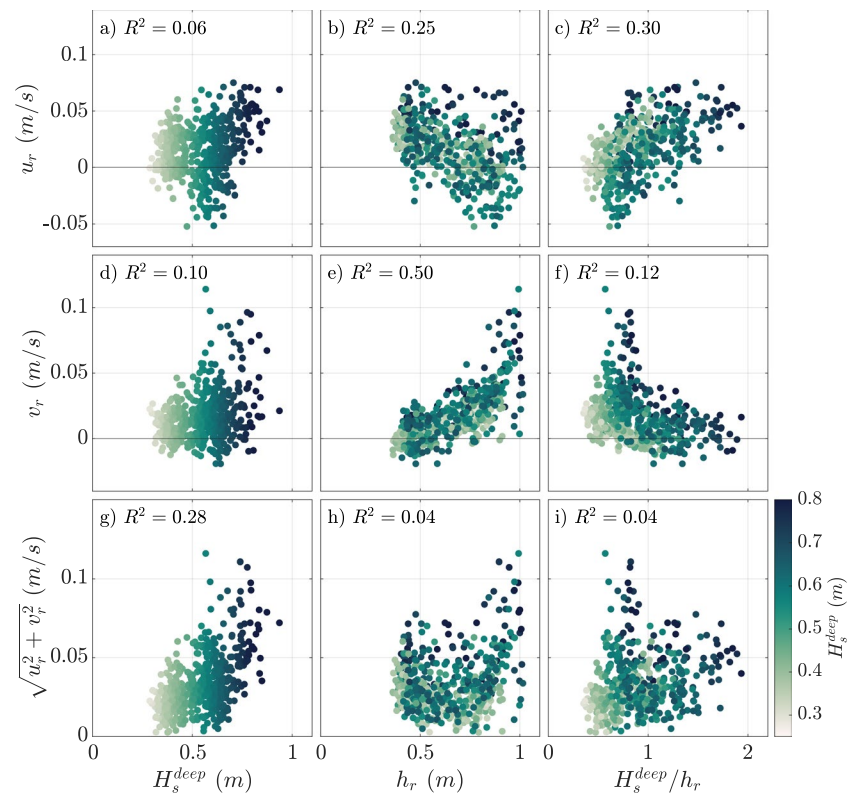
Figure 4. Observations from D-4. Upper row: Cross-reef velocity (u_r) compared to (a) wave heights, (b) depth on the reef flat, and (c) the ratio of offshore wave height to depth on the flat. Middle row: Along-reef velocity (v_r) compared to (d) wave heights, (e) depth on the reef flat, and (f) the ratio of offshore wave height to depth on the flat. Bottom row: Velocity magnitude ($\sqrt{u_r^2 + v_r^2}$) compared to (g) wave heights, (h) depth on the reef flat, and (i) the ratio of offshore wave height to depth on the flat. Colors indicate offshore wave heights H_s^{deep}.

4. Numerical Modeling of Idealized Reefs

4.1. Model Configurations

We present two model geometries, set up in Delft3D 4 with structured grids (Deltares, 2014). The model bathymetry configurations are shown in Figure 5, and the characteristics are listed in Table 2. All models are run 2DH (depth averaged) with a single vertical layer. The fringing reef model is based on an idealized geometry of the reef in Ofu, American Samoa (Figures 5a and 5b). Each reef flat has dimensions 904×112 m, the channels are 88 m wide, and the pool is 192 m wide. The fore reef has a 1/25 slope, and a drag coefficient of $C_D = 0.01$ is set for the entire domain. Rosman and Hench (2011) reported drag coefficients from multiple studies to span the range $C_D \sim \mathcal{O}(0.001 - 0.1)$. We set the mean depth and tidal range to $h_0 = 0.6$ m and $a = 0.5$ m for all fringing reef model runs, and vary the wave height at the boundary. Circulation cells are generated in this geometry where waves force flow over the flat, through the pool, and out of the channel. To minimize the effects of the lateral boundaries and allow for this flow pattern to establish, we include four channels and study the circulation in the area between the two inner channels. The fringing reef has three closed boundaries (two lateral and one shoreward) and one open boundary with a tidal water level boundary condition. The model is forced with an online coupled FLOW/WAVE model using Simulating WAves Nearshore (SWAN; Booij et al., 1999) and a Joint North Sea Wave Project (JONSWAP) wave spectrum with incident waves normal to the shore. Offshore significant wave heights are varied between 0.1 and 3.5 m. Breaking is modeled using the Battjes and Janssen (1979) model. Model parameters are given in Table 2.

The barrier reef is similar to the fringing reef, except the leeward side of the bathymetry is mirrored around the vertical axis such that instead of having a shallow pool, the depth increases away from the flat
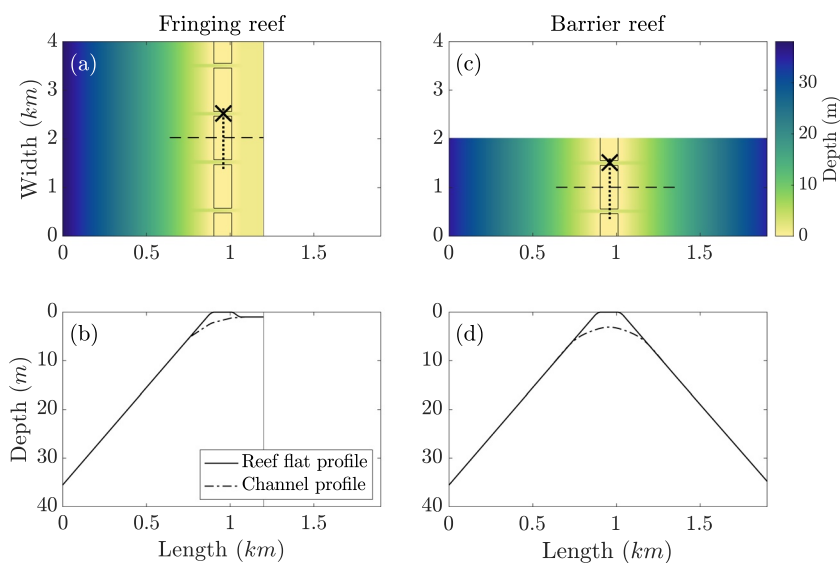
Figure 5. Bathymetry of the two numerical models. Left column shows the fringing reef bathymetry, right column shows the barrier reef bathymetry. In (a) and (c), the dashed line indicates the cross-reef transect in Figures 9 and 7, and the dotted line indicates the along-reef transect locations. Model results of channel velocities are evaluated at X. The solid line indicates the location of the reef flat. In (b) and (d) the solid line is the bathymetry over the length of the domain over the reef flat, and the dash-dotted line is the bathymetry over the length of the domain through the channel.

Table 2

Numerical Model Parameters

Grid resolution (FLOW & WAVE grids)	8×8m
Reef flat width (Δx)	112 m
Reef flat length	904 m
Lagoon width (fringing reef only)	192 m
Channel width	88 m
Fore-reef slope	1/25
Drag coefficient (C_D)	0.01
Mean still water depth on reef flat (h_0)	0.6 m
Tidal amplitude (a)	0.5 m
Tidal period	12 h
Wave boundary parameterization	JONSWAP
Offshore significant wave heights (H_s)	0.1–3.5 m
Peak wave period (T)	10 s
Peak enhancement factor	3.3
Wave direction	Shore-normal
Wave breaking	Battjes and Janssen (1979)
Alpha coefficient for wave breaking (α)	1
Breaking parameter (γ)	0.35
Wave bed friction	JONSWAP
Wave bed friction coefficient	0.067 m^2/s^3

Abbreviation: JONSWAP, Joint North Sea Wave Project.

(Figures 5c and 5d). For this reason, the barrier reef is longer than the closed reef. Additionally, the barrier reef is narrower than the fringing reef as the flow is almost entirely along the *x*-axis, and we do not need to take into account any return flow circulation. The barrier reef (Figure 5a and 5b) is symmetric around the vertical axis, with a 1/25 sloping fore reef, a shallow, horizontal reef flat of same dimensions as the fringing reef flats, and a 1/25 slope leeward of the flat. Coral reef slopes vary significantly between sites, from 1/50 in Lowe et al. (2005) studying Kaneohe Bay in Hawai'i, to a 1:1 slope in Storlazzi et al. (2018) in Faga'alu Bay, American Samoa. We ran models with 1/40 and 1/10 slopes for comparison (not shown), and found that the flow magnitude varies between them; steeper fore-reef slopes create larger wave setup and drive stronger flows. However, in terms of describing the overall nature of the dynamics of the system we found no significant difference, and present only the 1/25 slope cases here. Buckley et al. (2014) found that SWAN was capable of predicting sea-swell wave heights on steeply sloping environments such as coral reefs, using a slope of 1/10.6, while it was unable of capturing spectral transformation of wave energy and infragravity wave heights. SWAN was found to under-predict setup slightly compared to observations. The barrier reef model has closed lateral boundaries, and identical up and downstream harmonic water level boundary conditions representing the tide.

4.2. Numerical Results: Fringing Reef Model

Considering the scenario where $H_s = 1$ m, Figure 6 shows streamlines of the flow during high tide (top) and low tide (bottom) on the middle reef flat in Figure 5a. The reef flat is the black-framed rectangular area centered in the figures. Similar to observations (see Figure 2), there is a
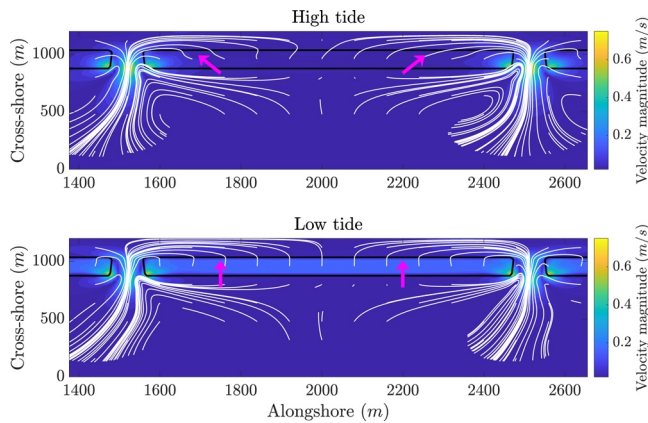
Figure 6. Example of Lagrangian velocity magnitudes (contour plot) and streamlines for the fringing reef model with parameters $H_s = 1$ m, $a = 0.5$ m, $h_0 = 0.6$ m, and $C_D = 0.01$ on high tide (top) and low tide (bottom). The solid black lines indicate the location of the reef flat. $x = 0$ is offshore.

distinct circulation pattern: Over the reef flat, into and along the pool, and out the channels. There are two particular differences between high and low tide: The magnitude and direction of flow on the flat. On low tide, the flow is nearly perpendicular to the crest (pink arrows) and the magnitude is larger than it is on high tide, where the flow is oblique to the crest, similar to the observations in Section 3. The largest velocities are observed near the channels, and the velocity in the channel and on the reef flat are out of phase; on high tide, the velocity over the reef flat is smallest and the velocity in the channels is the largest, and vice versa on low tide. Figure 7 shows the cross-reef momentum terms on high and low tide.

On the fore reef, a typical pressure gradient-radiation stress gradient balance is established as waves break, creating wave setup. The maximum setup occurs on low tide, qualitatively similar to the Tait (1972) expression where $\Delta \eta \propto h_b - h_r$, meaning the larger the difference between the depth at breaking and the depth on the flat, the larger the setup. In spite of this, the dynamics on the fore reef vary minimally between high and low tide. The major difference between the two simulation results is observed on the reef flat. On low tide (Figure 7, right column) radiation stress gradients are negligible on the flat, and a classic open channel flow balancing the pressure gradient and friction drives the flow over the reef flat perpendicular to the crest. Low tide is also when the largest reef flat
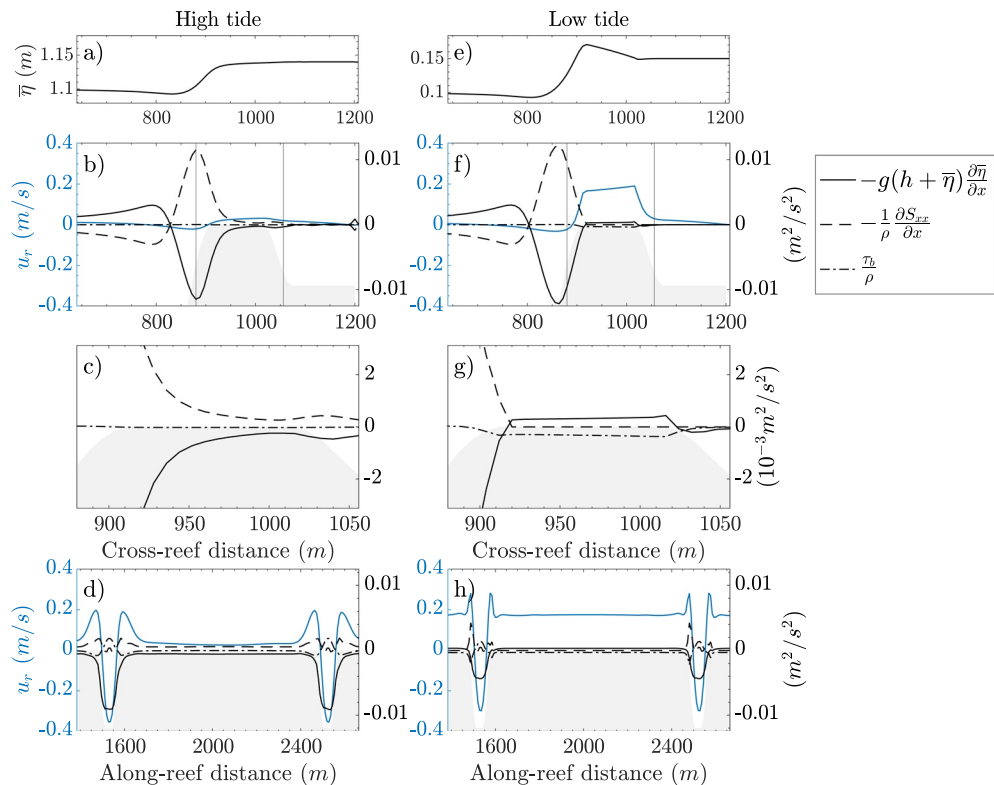

Figure 7. Fringing reef model results, where $a = 0.5$ m, $h_0 = 0.6$ m, and $H_s = 1$ m. Cross-reef results are evaluated along the dashed line in Figure 5a, and along-reef results are evaluated along the dotted line. (a) and (e) show the water level on high and low tide. (b) and (f) show the depth-integrated, cross-reef momentum terms and velocity on high and low tide evaluated cross reef. The vertical lines correspond to the length of reef plotted in (c) and (g). (c) and (g) are the same as (b) and (e), focused on the reef flat. (c) and (f) show the depth-integrated, cross-reef momentum terms and velocity on high and low tide evaluated along reef. Gray area represents bathymetry (no scale).
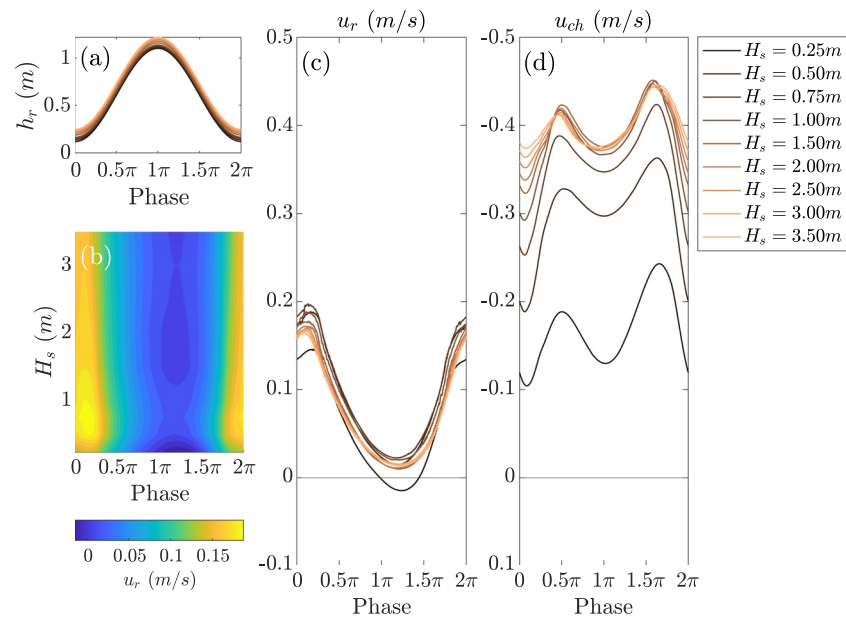
Figure 8. Fringing reef model results. (a) Water level on the reef flat, (b) contour plot of cross-reef velocity for all simulations, (c) cross-reef velocity, and (d) channel velocity. (b) is a contour plot of (c).

velocities are observed, and when the reef is most similar to an open reef. On high tide (Figure 7, left column), an onshore-directed radiation stress gradient balances an offshore pressure gradient, with negligible friction. This balance is expected on a beach, or what we here call a closed reef. This beach-like dynamic is reflected in the small cross-reef velocities in Figure 7b. Figures 7d and 7h show the force balance the along-reef direction, and illustrates the effect of the channels. Close to the channels the cross-reef flow is enhanced. As expected, the largest velocities are observed in the channel itself, directed offshore. Simultaneously, water adjacent to the channels is entrained creating a counter current and strong shear. The resulting cross-shore flow as a function of tidal phase is shown in Figure 8, where we summarize multiple simulation runs with varying offshore wave boundary conditions. Figure 8a shows the water level on the reef flat, (b) and (c) the cross-reef velocity, and (d) the channel velocity.

Our numerical modeling results confirm the out of phase nature of the reef flat and channel velocities shown in the observations. In general, increasing offshore wave heights increase the flow out of the channel, to a limit. Interestingly, this is not the case for the cross-reef flow, which seems to decrease for larger wave heights. Maximum cross-reef flows are found when $H \approx 0.7$ m. We interpret this as a consequence of the reef being closed. As the reef becomes more closed (and more beach-like), the wave setup relative to the pool setup decreases as does the onshore pressure gradient, which ultimately reverses. This condition is most apparent in the high tide fringing reef case.

4.3. Numerical Results: Barrier Reef Model

Figure 9 gives an example of the depth-integrated cross-reef momentum terms, water depth, and velocities at high and low tide, with the same forcing as the fringing reef model in Figure 7. Similar to the fringing reef model, the largest setup is observed on low tide. The corresponding radiation stress gradient term and opposing pressure gradient term are larger on low tide than on high tide due to increasing depth-limited breaking. However, contrary to the fringing reef model, cross-reef currents are stronger on high tide despite the smaller setup, as the depth-integrated pressure gradient term is larger on high tide. On both high and low tide, radiation stress gradients are negligible on the reef flat itself, where the pressure gradient and friction balance to drive a cross-reef flow. This is what we define as an open reef. The inclusion of the two channels creates along-reef variability, the effect of which is only observed relatively close to the channels themselves, as shown in Figures 9d and 9h, and for the majority of the reef flat we assume a 1D cross-reef momentum balance. The influence of the channel on the dynamics is observed approximately 100 m from
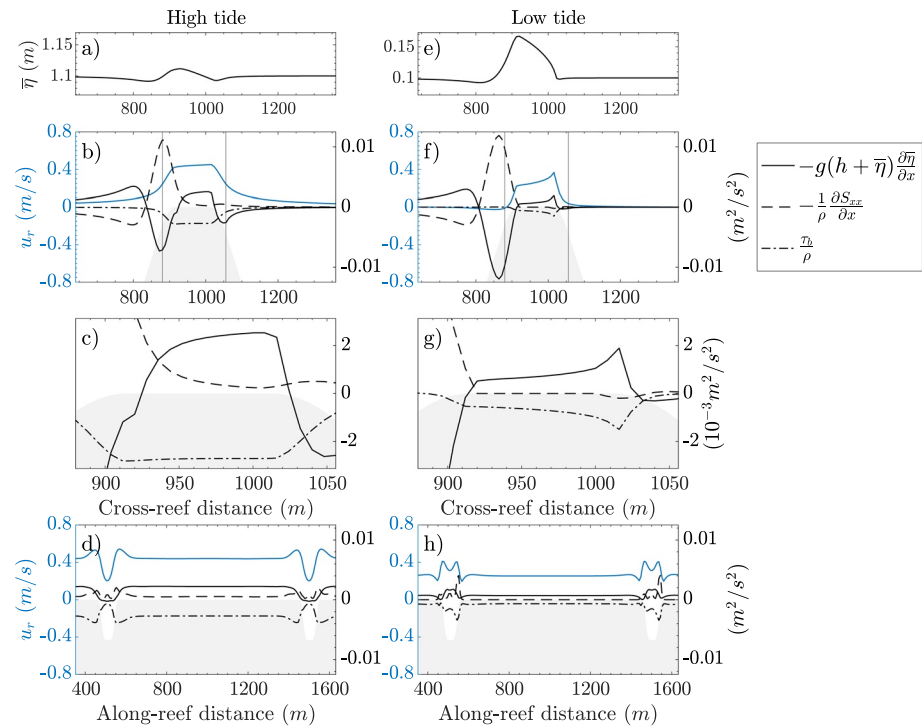
Figure 9. Barrier reef model results, where $a = 0.5$ m, $h_0 = 0.6$ m, and $H_s = 1$ m. Cross-reef results are evaluated along the dashed line in Figure 5c, and along-reef results are evaluated along the dotted line. (a) and (e) show the water level on high and low tide. (b) and (f) show the depth-integrated, cross-reef momentum terms and velocity on high and low tide evaluated cross reef. The vertical lines correspond to the length of reef plotted in (c) and (g). (c) and (g) are the same as (b) and (e), focused on the reef flat. (d) and (h) show the depth-integrated, cross-reef momentum terms and velocity on high and low tide evaluated along reef. Gray area represents bathymetry (no scale).
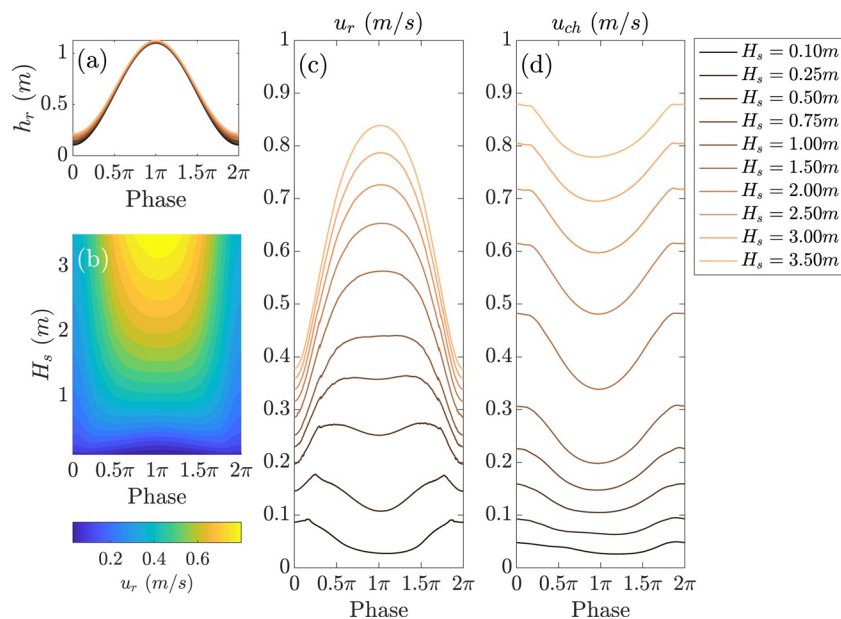

Figure 10. Barrier reef model results. (a) Water level on the reef flat, (b) contour plot of cross-reef velocity for all simulations, (c) cross-reef velocity, and (d) channel velocity. (b) is a contour plot of (c).

the channel itself. Our results show that along-reef advection and radiation stress gradient terms become increasingly important close to the channel, but can be neglected on the majority of the reef flat.

To study how the open reef flow responds to varying wave heights, we run the same model with a number of different offshore wave boundary conditions, see Figure 10. Consistently, velocities increase with increasing wave heights, and the phase of the flow varies from having two maxima per tidal cycle for smaller wave heights to a single maximum for larger waves. Figure 10 is what we expect from classic 1D reef models, where velocities increase with offshore wave heights and tides, and we observe higher harmonic behavior as first described by Symonds et al. (1995). In Section 5, we examine this dynamic in more detail, and explain the change in phase observed in Figure 10c.

4.4. Synthesis

Based on our definition of open and closed reefs, we can cast all of the model results presented above in terms of the two ratios $\left| \dfrac{g(h+\bar{\eta})\dfrac{\partial\bar{\eta}}{\partial x}}{C_d u\,|u|} \right|$ and $\left| \dfrac{g(h+\bar{\eta})\dfrac{\partial\bar{\eta}}{\partial x}}{\dfrac{1}{\rho}\dfrac{\partial S_{xx}}{\partial x}} \right|$. When the first or second term approaches unity, the reef behaves as an open or closed reef, respectively. Thus, as seen in Figures 11 and 12, the three asymptotic behaviors in the cross-reef dynamics emerge: Open, closed, and a transition area where the pressure gradient is close to zero.
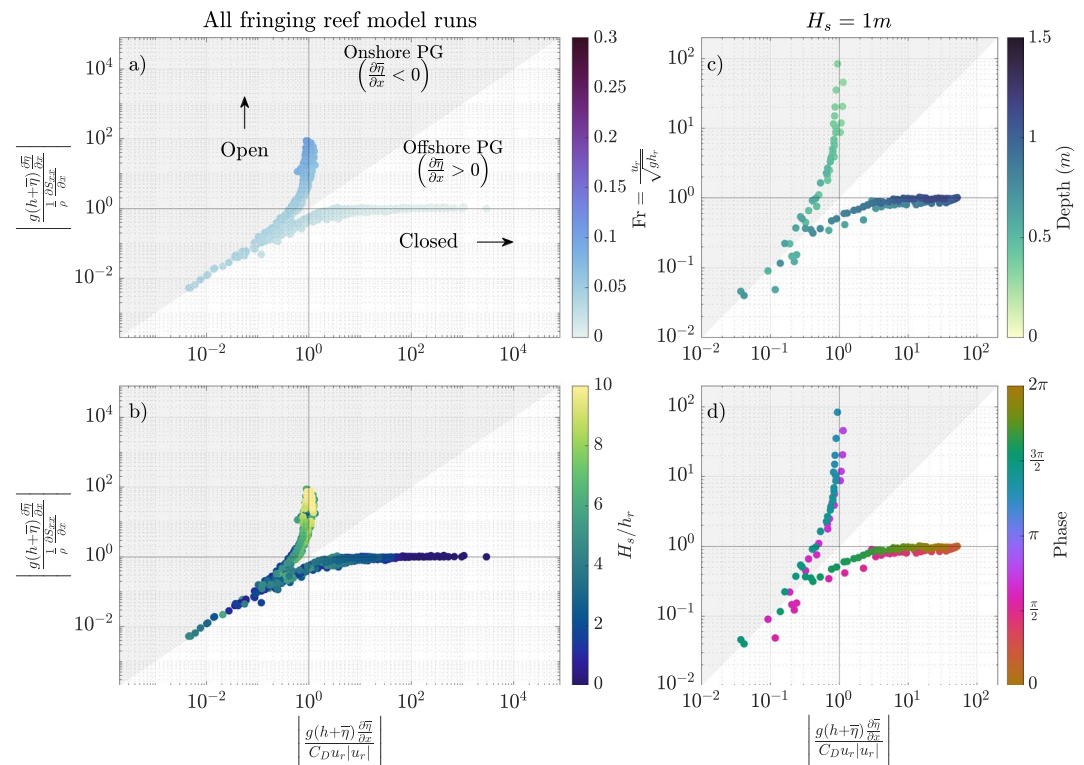

Figure 11. Fringing reef numerical model results. The magnitude of the pressure gradient term relative to the friction term is on the horizontal axis and the magnitude of the pressure gradient term relative to the radiation stress gradient term on is the vertical axis. All three terms are evaluated in the same place, halfway across the reef flat. The gray area coincides with onshore pressure gradients (similar to open channel flow), and the white area with offshore pressure gradients (similar to beach dynamics). (a) Scatter plot of the Froude number for all fringing reef model runs. PG: Pressure gradient. (b) Scatter plot of H_s/h_r, the ratio of the deep-water significant wave height to the depth on the reef flat. (c) Scatter plot of the depth h_r on the reef flat for the case $H_s = 1$ m. (d) Scatter plot of the phase of the $H_s = 1$ m case.

As the reef transitions from closed to open, the Froude number on the reef flat increases, as does the ratio H_s/h_r, the deep-water significant wave height relative to the total depth on the reef flat. Larger wave heights or shallower reef flats trend toward an open reef, and smaller wave heights or deeper reef flats trend toward a closed reef. Defining this fringing reef as closed based on geometry alone is not particularly helpful as it is dynamically similar to a barrier reef, or an open reef, on low tide. Still water level and wave conditions dictate whether or not the flow on the flat is impeded by the geometry. In contrast, the barrier reef model behaves as an open reef throughout in all model runs, except the short periods where the depth on the flat is too large to initiate wave breaking on the fore reef or reef crest.

Figures 11c and 11d show the evolution of the flow through the tidal cycle with $H_s = 1$ m offshore: Starting at low tide, the cross-shore dynamics are governed by a pressure gradient-friction balance, cross-shore velocities are maximum, and the system is an open reef. On the rising tide, the onshore pressure gradient relaxes due to decreasing depth-limited wave breaking. The pressure gradient changes sign about halfway through the tidal cycle, and is now offshore on high tide. As the cross-reef velocities decrease, so does the friction term, and the offshore pressure gradient is balanced by an onshore radiation stress gradient, becoming closed.

The reef flat Froude number increases as the depth decreases. On low tide and large offshore wave heights, the Froude number approaches a maximum of $Fr \approx 0.3$. The open-reef flow could potentially become supercritical under certain conditions, in which case the analysis here as either open or closed may not be applicable. None of our model runs produced $Fr \approx 1$, however, using numerical models and observations, Sous et al. (2020) found that such a critical regime is indeed possible, with supercritical flow and the occurrence of hydraulic jumps dependent on phase-resolved wave dynamics, which are not represented in Delft3D and SWAN. Thus, study of the supercritical regime could be an interesting avenue for future work.

5. A Simplified Model of Open Reef Dynamics

5.1. The One-Dimensional Model

The dynamics of open reefs, as typified by barrier reefs (Gourlay, 1996a) can be explored using a 1D model (Symonds et al., 1995). Due to the relatively simple behavior of this configuration, it is possible to develop analytical expressions to determine the cross-reef flow. Here, we present a simple model based on previous work by Symonds et al. (1995) that focuses on explaining observed flow variability caused by variations in both tidal water level and wave forcing. Notably, a key parameter governing open reef dynamics is the relative depth at breaking, h_b/h, which can predict phase and magnitude of the current on the reef flat. A key assumption is the use of the simple breaking model defined by a single constant γ as opposed to more complicated variants like that of Battjes and Janssen (1979).

On the reef flat of an open reef with negligible along-reef variability (Figure 1a), we can describe the 1D system by

$$g(h + \overline{\eta})\frac{\partial \overline{\eta}}{\partial x} = -\frac{\tau_b}{\rho}.$$

We assume a quasi-stationary flow, that is, we allow the depth to vary on a tidal time scale while the pressure gradient-friction balance adjusts instantaneously. Incident waves break on the fore reef which creates a wave-induced setup on the reef flat that drives a flow balanced by friction, a behavior shown in our numerical simulations. Radiation stress gradients are negligible downstream of the surf zone (Lentz et al., 2016; Monismith, 2007; Symonds et al., 1995), which we assume occupies part of the fore reef and ceases at the reef crest. The setup downstream of the reef is small compared to the setup on the reef flat. This reef type has been studied in the field by Lentz et al. (2016) and Monismith et al. (2013) among others.

Given the complexity of estimating wave setup on reefs *a priori*, we assume that there exists some coefficient Γ for a particular reef, such that the setup can adequately be estimated as $\Delta\eta \approx \Gamma(h_b - h_r)$, according to Tait (1972). We assume the setup decreases linearly over the reef, which presupposes a constant drag coefficient, negligible radiation stress gradients, and a horizontal reef flat. Based on our simulations, Figure 9,
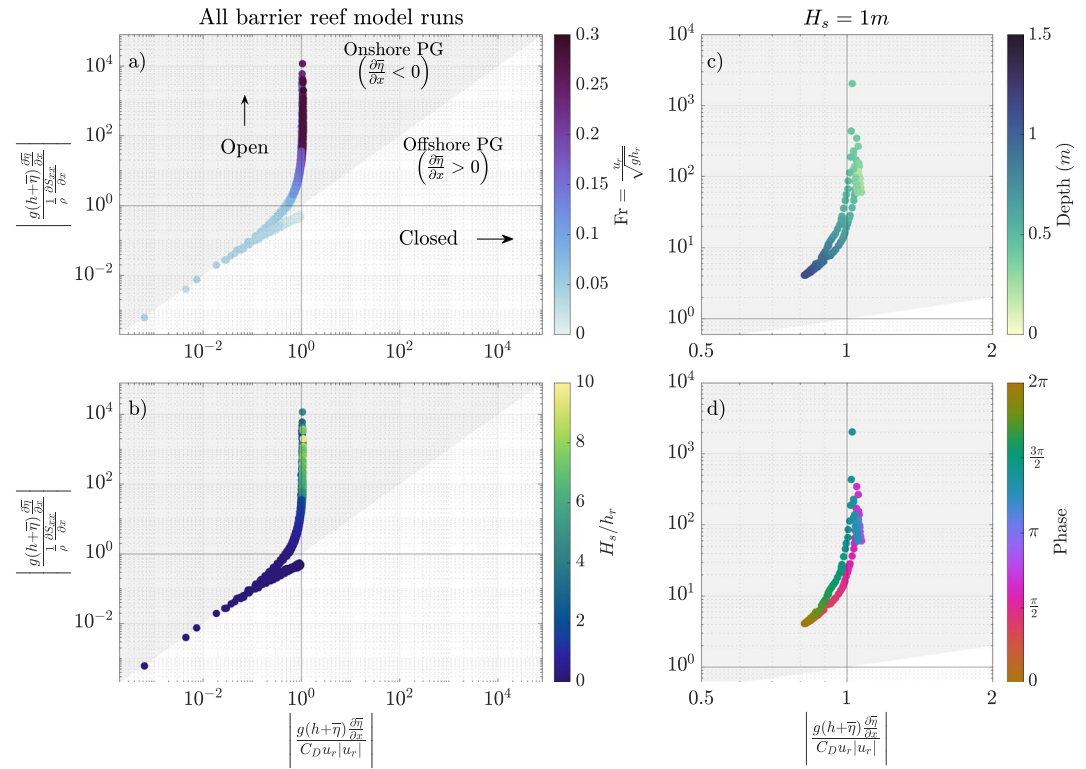
Figure 12. Barrier reef numerical model results. Same axis as Figure 11. (a) Scatter plot of the Froude number for all barrier reef model runs. PG: Pressure gradient. (b) Scatter plot of H_s/h_r, the ratio of the deep-water significant wave height to the depth on the reef flat. (c) Scatter plot of the depth h_r on the reef flat for the case $H_s = 1$ m. (d) Scatter plot of the phase of the $H_s = 1$ m case.

this is a reasonable assumption. The tidally varying depth on the reef flat, h, is expressed as a harmonic function

$$h = a\sin(\omega t) + h_0, \tag{4}$$

where a is the tidal amplitude, ω is the tidal angular frequency ($\omega = 2\pi/T$, where T is the tidal period), and h_0 is the mean water depth. Then the total depth on the reef flat is

$$h_r = h + \overline{\eta}. \tag{5}$$

The water level gradient across the reef is, using Equation 2

$$\frac{d\overline{\eta}}{dx} \approx -\frac{\Delta\eta}{\Delta x} = -\frac{\Gamma}{\Delta x}\left(h_b - h - \Delta\eta\right),$$

or

$$-\frac{\Delta\eta}{\Delta x} = -\frac{\Gamma}{\left(1 + \Gamma\right)\Delta x}\left(h_b - h\right),$$

where Δx is the width of the reef, and we define $\Gamma' = \dfrac{\Gamma}{\Gamma + 1}$. The cross-reef pressure gradient halfway across the reef flat is

$$F_P = -g\left(h + \Gamma'\frac{(h_b - h)}{2}\right)\frac{\Gamma'}{\Delta x}\left(h_b - h\right). \tag{6}$$

Combining Equations 4–6, this pressure gradient force term can be written with terms that vary at the tidal frequency ω, and at twice the tidal frequency 2ω, as well as a mean term

$$F_P = F_\omega \sin(\omega t) + F_{2\omega} \cos(2\omega t) + F_0, \tag{7}$$

where

$$F_\omega = \frac{ag\Gamma'}{\Delta x}\Big[\big(\Gamma' - 2\big)h_0 + \big(1 - \Gamma'\big)h_b\Big], \tag{8}$$

$$F_{2\omega} = \frac{a^2 g\Gamma'}{2\Delta x}\left(1 - \frac{\Gamma'}{2}\right), \tag{9}$$

$$F_0 = \frac{g\Gamma'}{\Delta x}\left[\frac{\Gamma'}{2}h_b^2 + \big(1 - \Gamma'\big)h_0 h_b + \left(\frac{a^2}{2} + h_0^2\right)\left(\frac{\Gamma'}{2} - 1\right)\right]. $$

Assuming a pressure gradient-friction balance with a quadratic friction term, $\tau_b/\rho = C_D u_r|u_r|$, the cross-reef Eulerian velocity is

$$u_r = \sqrt{\frac{F_P}{C_D}}. \tag{10}$$

where C_D is the drag coefficient, which we assume is spatially invariable and does not depend on the depth. Note that since we are examining the flow on the reef flat, we assume that waves are small due to the shallow depth and depth-induced breaking on the reef flat. We can therefore estimate the friction in terms of the mean Eulerian velocity without taking into account enhancement of drag due to waves (Lentz et al., 2018). Critically, per the derivation, the flow is always positive on this reef (directed from the reef crest where wave breaking takes place). Symonds et al. (1995) predicted that the higher harmonics of reef flows would only occur when a certain threshold of the tidal amplitude was exceeded. In contrast, our analysis shows that the cross-reef velocity includes a term with twice the tidal frequency, and the higher harmonic is an intrinsic manifestation of a non-linear pressure gradient term. We expect higher harmonics on all reefs where tidally modified wave breaking takes place.

We can find the maximum flow across the reef as a function of the phase of the tide, by taking the derivative of u_r with respect to still water depth h and equating it to zero, giving

$$2\Gamma' gh - \Gamma' gh_b - (\Gamma')^2 gh + (\Gamma')^2 gh_b = 0,$$

or

$$\frac{h_b}{h} = \frac{2 - \Gamma'}{1 - \Gamma'} = \alpha. \tag{11}$$

For $\gamma = (0.3, 1)$, $\Gamma' \approx (0.04, 0.2)$ (using Equation 2), and we calculate $\alpha \approx 2$–2.3. Given that Equation 2 often over predicts wave setup on reefs (Gourlay, 1996a; Lowe et al., 2009), Γ' is likely even smaller and the approximation $\alpha \approx 2$ holds. Hence, the maximum cross-reef flow occurs when $h_b \approx 2h$. Figure 13c shows the solution to Equation 10 for a given set of parameters over one tidal period. Varying the incident wave height, we evaluate the depth-averaged velocity as a function of tidal phase (Figure 13b). In the case of the smallest wave heights, only an intermittent cross-reef flow exists, since no waves break on high tide. This creates a velocity signal in opposite phase of the tide. As incident wave heights increase, so does the cross-reef flow. If $h_b/h > \alpha$ throughout the tidal period, the largest cross-reef flow coincides with the highest tide, and the flow is in phase with the tide, and vice versa. Compare to the results from the numerical barrier reef model, Figure 13d.

Furthermore, the phase of the cross-reef flow depends on F_ω (Equation 8). If F_ω changes sign, this is equivalent to a change in phase since $-\sin(\theta) = \sin(\theta + \pi)$. Hence, $F_\omega = 0$ when
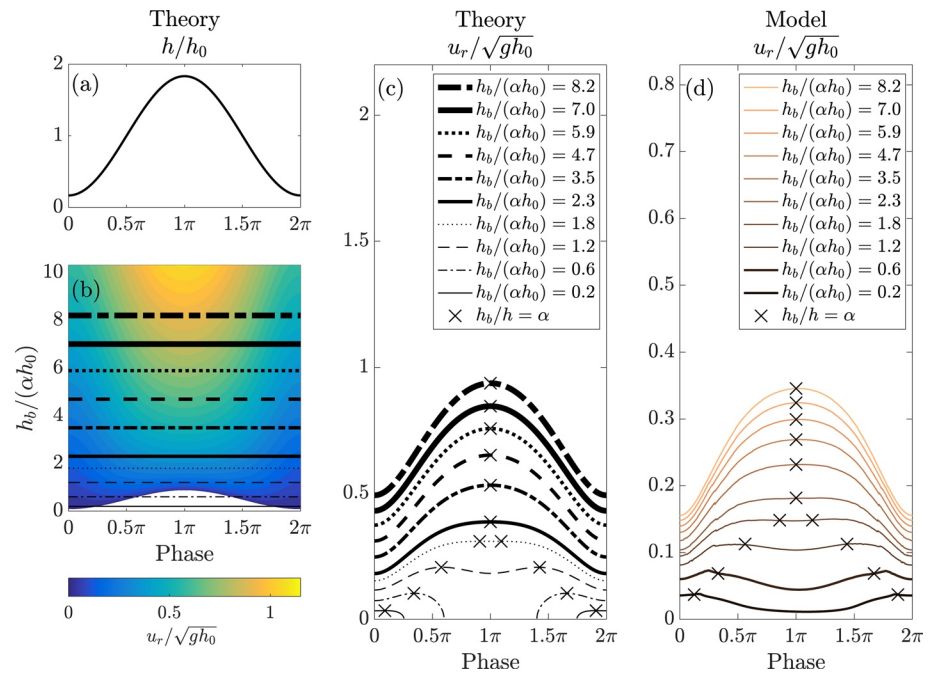
Figure 13. (a) Tidal water depth on the reef flat given $h_0 = 0.6$ m and $a = 0.5$ m (Equation 4), nondimensionalized by h_0. (b) Depth-averaged, cross-reef velocities as a function of nondimensionalized depth at breaking $h_b/(\alpha h_0)$ and tidal phase, calculated from Equation 10, with parameters $\Delta x = 100$ m, $\gamma = 0.35$, and $C_D = 0.01$. Here, Γ' is estimated using the Tait (1972) expression, Equation 2. The white area indicates $u_r = 0$ as no depth-limited breaking takes place. Velocities are nondimensionalized by $u_r / \sqrt{gh_0}$. (c) Depth-averaged, cross-reef velocities for select values of h_b. Each horizontal black line corresponds to the black line of similar formatting in (b). The markers show $h_b/h = \alpha$, when the maximum velocity occurs. (d) Same as (c) but for the barrier reef numerical model, repeated from Figure 10.

$$\frac{h_b}{h_0} = \frac{2 - \Gamma'}{1 - \Gamma'} = \alpha.$$

Using this expression, we can predict whether high tide or low tide will experience larger velocities. In terms of the mean depth h_0, if the depth at breaking $h_b > h_0\alpha$, the velocity is larger on high tide than on low tide ($F_\omega > 0$), and vice versa ($F_\omega < 0$) if $h_b < h_0\alpha$. If $h_b = h_0\alpha$, the flow phase is entirely expressed through the higher harmonic $F_{2\omega}$ in Equation 9.

5.2. Importance of Relative Depth at Breaking

The analysis given above shows that maximum cross-reef velocities should occur when $h_b/h = \alpha \approx 2$, and that the ratio $h_b/(h_0\alpha)$ determines whether the maximum cross-reef flow occurs on high tide or low tide. Both of these results are corroborated in work by Bonneton et al. (2007) from observations in New Caledonia. Bonneton et al. (2007) employ a similar analysis, and show that during the first 7 days of their two-week deployment, $h_b/h = 2$ twice daily, producing twice daily maximum flows. On the latter half of the deployment $h_b/h < 2$, and the flow was out of phase with the tide, as predicted by our model. Both Gourlay and Colleter (2005) and Symonds et al. (1995) found similar criteria.

5.3. Limitations of the Theoretical Model

Unlike what the simple theory given above predicts, the computed flow is never exactly zero, since the incident wavefield in our model uses the JONSWAP wave spectrum so some wave breaking takes place no matter how small the offshore significant wave height. More importantly, while the theoretical model can be used to predict the phase of the cross-reef flow relative to the tide, and whether one or two daily maxima

are expected, as seen in Figure 13, the theoretical flow is 2–3 times larger than the modeled flow. The overestimation of flow magnitude is likely due to the fact that the theory is based on using a constant value of Γ to represent breaking, whereas the numerical model uses the more complex model of Battjes and Janssen (1979). In contrast, the discrepancy between observed and predicted values of setup reported by Lowe et al. (2009), was likely due to the fact that a value of Γ *a priori* was chosen. Indeed, while not truly predictive, simple analytical expressions such as Equation 2 (albeit cast in terms of energy flux) can be accurately fitted to field observations so as to determine Γ (Monismith et al., 2013; Vetter et al., 2010). In a similar fashion, comparing model results to laboratory experiments on wave breaking and setup, Buckley et al. (2014) found that both SWAN and the free surface solver SWASH (Smit et al., 2014) could provide accurate predictions of setup given appropriate values of the parameters used by their respective wave breaking models.

Another limitation of our simplified model is the case in which the Froude number exceeds 1, a behavior our model does not account for but has been observed by Sous et al. (2020). If the cross-reef velocity is nondimensionalized by $u_r / \sqrt{gh_r}$, using the instantaneous depth not the mean depth, Figure 13b and 13d would present the Froude number on the flat (not shown here). If $Fr > 1$, a hydraulic jump might occur on the reef flat, which is clearly not captured in the preceding discussion, and the cross-reef surface slope would not be constant. While our theory would not apply to such a case, it still could be used to predict under what flow conditions the reef flat would become supercritical.

6. Conclusion

Based on observations and numerical methods, we identify two distinct cross-reef dynamical regimes on coral reefs, and classify them as open and closed. Open reefs are characterized by a cross-reef pressure gradient-friction balance, and experience strong cross-reef flows. Closed reefs are characterized by a cross-reef pressure gradient-radiation stress gradient balance, with cross-reef flows reduced and along-reef flows increased. The distinction is useful as the responses to changes in forcing by waves and tides differ between the two regimes.

Previous classification of reefs and lagoons as open or closed can be ambiguous as it often is based on geometry which is an insufficient predictor of reef hydrodynamics. The reef systems of Kaneʻohe Bay and the north shore of Moorea are geometrically similar, yet behave very differently, with Kaneʻohe Bay appearing nearly closed (Lowe et al., 2009) while the Moorea reef appears to be nearly open (Monismith et al., 2013). The observations from Ofu in America Samoa (Maticka, 2019) provide an example of a reef which is closed on high tide, but open (and thus similar to a barrier reef) on low tide. Judging by the geometry alone, it could be classified as closed as it is a fringing reef or open due to channel incisions, but either would entirely miss the tidally alternating behavior between two very different dynamical regimes. It follows that the classification suggested here is not an absolute designation of a given reef, but rather a description of the dominant dynamics. A reef might transition from one dynamical type to another depending on wave and tidal conditions. Additionally, changes in bathymetry, bottom roughness, and still water level due to, for example, reef growth or degradation, dredging, or storm damage could potentially shift a given reef from one dynamical regime to another.

In addition to our fringing reef model, we show results from a barrier reef with open-reef dynamics. Balancing the pressure gradient and friction on the reef flat, we show that the velocities are proportional to offshore wave heights, in agreement with both observations and previous studies. We explain an often observed higher harmonic in cross-reef velocities in terms of non-linear interactions between wave setup and a tidally varying water depth, and show how the phasing of the flow depends on both offshore wave conditions and tides. The fundamental challenge in matching analytical solutions to observations and numerical models lies in accurately predicting the magnitude of wave setup on reefs, which is the main forcing mechanism of flow on both open and closed reefs. Given that setup is strongly dependent on wave breaking, it is clear that improved predictive models of flows on reefs requires improved models of wave breaking.

While we recognize that the suggested framework is descriptive, and cannot on its own predict the dynamical regime of a particular reef *a priori*, we believe that the present study advances the development of a comprehensive classification of coral reef hydrodynamics by clarifying what makes a reef either open or closed. This distinction may be important to connecting reef circulation response to variable forcing with

ecosystem health in a variety of ways. For example, open reefs that transport water away from the reef system might provide larvae to nearby reefs or islands, and thus be good locations for marine protected areas (Golbuu et al., 2012). Closed reefs, which tend to be more retentive, that is, have circulation patterns that are more closed, might appear more isolated from the standpoint of larval connectivity, and thus might not be useful as marine protected areas. Additionally, reduced flow rates lead to long flushing periods, which in turn may increase retention of pollutants. However, closed reefs may naturally experience wider ranges of temperature, and thus may have corals that are more resilient to heating shocks that might otherwise cause bleaching (Pineda et al., 2013). Thus, classifying reefs in terms of their dynamics may help with understanding multiple aspects of coral reef health and resilience, and thus aid management of these important marine ecosystems.

Data Availability Statement

The data used in this study can be accessed online at https://purl.stanford.edu/fw159cv5766.

References

Atkinson, M., Smith, S. V., & Stroup, E. D. (1981). Circulation in Enewetak Atoll lagoon1. *Limnology & Oceanography*, *26*(6), 1074–1083. https://doi.org/10.4319/lo.1981.26.6.1074

Battjes, J. A., & Janssen, J. P. (1979). Energy loss and set-up due to breaking of random waves. In Proceedings of the coastal engineering conference (Vol. 1, pp. 569–587). New York, NY: American Society of Civil Engineers. https://doi.org/10.9753/icce.v16.32

Becker, J. M., Merrifield, M. A., & Ford, M. (2014). Water level effects on breaking wave setup for Pacific Island fringing reefs. *Journal of Geophysical Research: Oceans*, *119*, 914–932. https://doi.org/10.1002/2013JC009373

Bonneton, P., Lefebvre, J. P., Bretel, P., Ouillon, S., & Douillet, P. (2007). Tidal modulation of wave-setup and wave-induced currents on the Aboré coral reef, New Caledonia. *Journal of Coastal Research*, *50*(SPEC. ISSUE 50), 762–766. https://doi.org/10.2307/26481686

Booij, N., Ris, R. C., & Holthuijsen, L. H. (1999). A third-generation wave model for coastal regions: 1. Model description and validation. *Journal of Geophysical Research*, *104*(C4), 7649–7666. https://doi.org/10.1029/98JC02622

Buckley, M., Lowe, R., & Hansen, J. (2014). Evaluation of nearshore wave models in steep reef environments. *Ocean Dynamics*, *64*(6), 847–862. https://doi.org/10.1007/s10236-014-0713-x

Callaghan, D. P., Nielsen, P., Cartwright, N., Gourlay, M. R., & Baldock, T. E. (2006). Atoll lagoon flushing forced by waves. *Coastal Engineering*, *53*(8), 691–704. https://doi.org/10.1016/j.coastaleng.2006.02.006

Deltares. (2014). *3D/2D modeling suite for integral water solutions: Delft3D hydro-morphodynamics user manual* (Technical Report). Delft: Deltares. Retrieved from https://content.oss.deltares.nl/delft3d/manuals/Delft3D-FLOW\text{_}User\text{_}Manual.pdf

Franklin, G., Mariño-Tapia, I., & Torres-Freyermuth, A. (2016). Effects of reef roughness on wave setup and surf zone currents. *Journal of Coastal Research*, *165*(65), 2005–2010. https://doi.org/10.2112/si65-339.1

Golbuu, Y., Wolanski, E., Idechong, J. W., Victor, S., Isechal, A. L., Oldiais, N. W., et al. (2012). Predicting coral recruitment in Palau's complex reef archipelago. *PloS One*, *7*(11), e50998. https://doi.org/10.1371/journal.pone.0050998

Gourlay, M. R. (1996a). Wave set-up on coral reefs. 1. Set-up and wave-generated flow on an idealized two dimensional horizontal reef. *Coastal Engineering*, *27*(3–4), 161–193. https://doi.org/10.1016/0378-3839(96)00008-7

Gourlay, M. R. (1996b). Wave set-up on coral reefs. 2. Set-up on reefs with various profiles. *Coastal Engineering*, *28*(1–4), 17–55. https://doi.org/10.1016/0378-3839(96)00009-9

Gourlay, M. R., & Colleter, G. (2005). Wave-generated flow on coral reefs-an analysis for two-dimensional horizontal reef-tops with steep faces. *Coastal Engineering*, *52*(4), 353–387. https://doi.org/10.1016/j.coastaleng.2004.11.007

Hearn, C. J. (1999). Wave-breaking hydrodynamics within coral reef systems and the effect of changing relative sea level. *Journal of Geophysical Research*, *104*(C12), 30007–30019. https://doi.org/10.1029/1999jc900262

Hefner, B. B., Rogers, J. S., Maticka, S. A., Monismith, S. G., & Woodson, C. B. (2019). Instrumentation for direct measurements of wave-driven flow over a fringing reef crest. *Limnology and Oceanography: Methods*, *17*(12), 627–638. https://doi.org/10.1002/lom3.10337

Hoeke, R. K., Storlazzi, C. D., & Ridd, P. V. (2013). Drivers of circulation in a fringing coral reef embayment: A wave-flow coupled numerical modeling study of Hanalei Bay, Hawaii. *Continental Shelf Research*, *58*, 79–95. https://doi.org/10.1016/j.csr.2013.03.007

Lentz, S. J., Churchill, J. H., & Davis, K. A. (2018). Coral reef drag coefficients-surface gravity wave enhancement. *Journal of Physical Oceanography*, *48*(7), 1555–1566. https://doi.org/10.1175/JPO-D-17-0231.1

Lentz, S. J., Churchill, J. H., Davis, K. A., Farrar, J. T., Pineda, J., & Starczak, V. (2016). The characteristics and dynamics of wave-driven flow across a platform coral reef in the Red Sea. *Journal of Geophysical Research: Oceans*, *121*(2), 1360–1376. https://doi.org/10.1002/2015jc011141

Longuet-Higgins, M. S., & Stewart, R. W. (1964). Radiation stresses in water waves; a physical discussion, with applications. *Deep-Sea Research and Oceanographic Abstracts*, *11*, 529–562. https://doi.org/10.1016/0011-7471(64)90001-4

Lowe, R. J., Falter, J. L., Bandet, M. D., Pawlak, G., Atkinson, M. J., Monismith, S. G., & Koseff, J. R. (2005). Spectral wave dissipation over a barrier reef. *Journal of Geophysical Research*, *110*(4), 1–16. https://doi.org/10.1029/2004JC002711

Lowe, R. J., Falter, J. L., Monismith, S. G., & Atkinson, M. J. (2009). A numerical study of circulation in a coastal reef-lagoon system. *Journal of Geophysical Research*, *114*(6), 1–18. https://doi.org/10.1029/2008JC005081

Lowe, R. J., Hart, C., & Pattiaratchi, C. B. (2010). Morphological constraints to wave-driven circulation in coastal reef-lagoon systems: A numerical study. *Journal of Geophysical Research*, *115*(9), 1–13. https://doi.org/10.1029/2009JC005753

Lowe, R. J., Leon, A. S., Symonds, G., Falter, J. L., & Gruber, R. (2015). The intertidal hydraulics of tide-dominated reef platforms. *Journal of Geophysical Research: Oceans*, *120*, 4845–4868. https://doi.org/10.1002/2015JC010701

Maticka, S. (2019). *A tale of two reefs: Hydrodynamics of a fringing reef & a reef atoll* (Unpublished doctoral dissertation). Stanford University.

Mei, C. C. (1983). The applied dynamics of ocean surface waves. *Ocean Engineering*, *11*. https://doi.org/10.1016/0029-8018(84)90033-7

Monismith, S. G. (2007). Hydrodynamics of coral reefs. *Annual Review of Fluid Mechanics*, *39*(1), 37–55. https://doi.org/10.1146/annurev.fluid.38.050304.092125

Monismith, S. G., Herdman, L. M. M., Ahmerkamp, S., & Hench, J. L. (2013). Wave transformation and wave-driven flow across a steep coral reef. *Journal of Physical Oceanography*, *43*(7), 1356–1379. https://doi.org/10.1175/jpo-d-12-0164.1

Pineda, J., Starczak, V., Tarrant, A., Blythe, J., Davis, K., Farrar, T., et al. (2013). Two spatial scales in a bleaching event: Corals from the mildest and the most extreme thermal environments escape mortality. *Limnology & Oceanography*, *58*(5), 1531–1545. https://doi.org/10.4319/lo.2013.58.5.1531

Raubenheimer, B., Guza, R. T., & Elgar, S. (1996). Wave transformation across the inner surf zone. *Journal of Geophysical Research*, *101*(C11), 25589–25597. https://doi.org/10.1029/96JC02433

Rogers, J. S., Maticka, S. A., Chirayath, V., Woodson, C. B., Alonso, J. J., & Monismith, S. G. (2018). Connecting flow over complex terrain to hydrodynamic roughness on a coral reef. *Journal of Physical Oceanography*, *48*(7), 1567–1587. https://doi.org/10.1175/JPO-D-18-0013.1

Rosman, J. H., & Hench, J. L. (2011). A framework for understanding drag parameterizations for coral reefs. *Journal of Geophysical Research*, *116*(8), C08025. https://doi.org/10.1029/2010JC006892

Smit, P., Janssen, T., Holthuijsen, L., & Smith, J. (2014). Non-hydrostatic modeling of surf zone wave dynamics. *Coastal Engineering*, *83*, 36–48. https://doi.org/10.1016/j.coastaleng.2013.09.005

Sous, D., Chevalier, C., Devenon, J.-L., Blanchot, J., & Pagano, M. (2017). Circulation patterns in a channel reef-lagoon system, Ouano lagoon, New Caledonia. *Estuarine, Coastal and Shelf Science*, *196*, 315–330. https://doi.org/10.1016/j.ecss.2017.07.015

Sous, D., Tissier, M., Bouchette, F., Dodet, G., & Rey, V. (2020). Extreme wave events on barrier reefs: A driver for critical regime? *Journal of Coastal Research*, *95*(sp1), 654–658. https://doi.org/10.2112/SI95-127.1

Storlazzi, C. D., Cheriton, O. M., Messina, A. M., & Biggs, T. W. (2018). Meteorologic, oceanographic, and geomorphic controls on circulation and residence time in a coral reef-lined embayment: Faga'alu Bay, American Samoa. *Coral Reefs*, *37*(2), 457–469. https://doi.org/10.1007/s00338-018-1671-4

Symonds, G., Black, K. P., & Young, I. R. (1995). Wave-driven flow over shallow reefs. *Journal of Geophysical Research*, *100*(C2), 2639–2648. https://doi.org/10.1029/94JC02736

Tait, R. J. (1972). Wave set-up on coral reefs. *Journal of Geophysical Research*, *77*(12), 2207–2211. https://doi.org/10.1029/jc077i012p02207

Thornton, E. B., & Guza, R. T. (1983). Transformation of wave height distribution. *Journal of Geophysical Research*, *88*(C10), 5925–5938. https://doi.org/10.1029/JC088iC10p05925

Vetter, O., Becker, J. M., Merrifield, M. A., Pequignet, A.-C., Aucan, J., Boc, S. J., & Pollock, C. E. (2010). Wave setup over a Pacific Island fringing reef. *Journal of Geophysical Research*, *115*(12), 1–13. https://doi.org/10.1029/2010JC006455